Int. J. Electron. Commun. (AEÜ) 177 (2024) 155153

Contents lists available at ScienceDirect

International Journal of Electronics and Communications

journal homepage: www.elsevier.com/locate/aeue

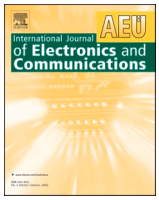

Regular paper

Indoor wireless channel characterization in the W band for the planning of 6G communication systems

Concepción Sanchis-Borrás [a,*], María-Teresa Martínez-Inglés [b], José-Víctor Rodríguez [c], José-Maria Molina-Garcia-Pardo [c,*]

[a] Universidad Católica de Murcia, Facultad Politécnica, 30107, Murcia, Spain
[b] Ministerio de Defensa-Universidad Politécnica de Cartagena, Centro Universitario de la Defensa San Javier, Departamento de Ingeniería y Técnicas Aplicadas, Spanish Air Force Academy 30720, Santiago de la Ribera, Spain
[c] Universidad Politécnica de Cartagena, Dpto. Tecnologías de la Información y las Comunicaciones, Antiguo Cuartel de Antigones, Plaza del Hospital, 1, 30202, Cartagena, Murcia, Spain

ARTICLE INFO

Keywords:
mMIMO
mmWave
60 GHz
94 GHz
Indoor communication
Channel modeling

ABSTRACT

This work presents a wireless channel characterization based on an extensive campaign of massive multiple-input multiple-output (mMIMO) measurements conducted under line-of-sight (LOS) conditions. These measurements focus on the 94 GHz band (W band), and the results are compared to the same positions measured at 60 GHz. The values of the relative received power, root mean square (RMS) delay spread, maximum excess delay (MED), and coherence bandwidth in an indoor laboratory environment are analyzed. The results of this study can contribute to a better understanding of the propagation channel behavior in the 94 GHz band, and can be used to assess the potential of this band for the upcoming sixth-generation (6G) networks in laboratory environments.

1. Introduction

In recent years, the demand for high-capacity wireless communication systems has surged, driven by the proliferation of data-intensive applications and the advent of the Internet of Things (IoT). To meet these burgeoning requirements, millimeter-wave (mmWave) frequencies have emerged as a promising frontier for wireless communication, as they offer the potential for multi-gigabit-per-second data rates [1]. The strong interest in mmWave frequencies over the last two decades has led to numerous measurement campaigns being conducted in indoor environments between the 1 GHz and 70 GHz frequency bands [2]. The authors of [3] presented a multidimensional measurement campaign in the range 75–110 GHz in an indoor environment, with the novelty that a commercial setup was modified by increasing the distance for one of the converters using precision coaxial cables and avoiding the use of amplifiers. In [4], measurements at 60 GHz were carried out in a laboratory. The work presented in [5] involved wideband channel measurements in an office environment in the 62 GHz and 83 GHz frequency bands.

Over the last five years, standardization authorities have been defining various frequency bands for the new generation of mobile communications. At the World Radio Conference 19 (WRC-19) [6], the 5G frequency bands for mmWave transmissions at 26 GHz (n258), 28 GHz (n257–261), 39 GHz (n260), 41 GHz (n259) and 47 GHz 31 (n262) were established. In [7], the 60 GHz band was presented as a band for sixth-generation (6G). In [8], frequencies in the range 90–300 GHz and the terahertz spectrum above 300 GHz were predicted as key enablers for 6G communication systems. In addition, at its meeting on June 23, ITU-R WP5D completed its recommendation framework for IMT-2030 (6G) [9]. Therefore, there is great interest in studying these frequencies for various application scenarios and in analyzing the channel characteristics. However, the main disadvantage of 6G is the high path loss due to the increase of carrier frequencies.

The 90 GHz band, with its abundant spectrum resources, offers tremendous promise for future indoor communication systems. Realizing the full potential of these frequency bands will necessitate a deep understanding of their behavior in indoor environments; however, to the best of our knowledge, there has been little research into the W band. Three decades ago, measurements at 94 GHz were carried out in [10] and [11], but the authors mainly focused on characterizing the

* Corresponding authors.
E-mail addresses: csanchis@ucam.edu (C. Sanchis-Borrás), mteresa.martinez@cud.upct.es (M.-T. Martínez-Inglés), jvictor.rodriguez@upct.es (J.-V. Rodríguez), josemaria.molina@upct.es (J.-M. Molina-Garcia-Pardo).

https://doi.org/10.1016/j.aeue.2024.155153
Received 13 December 2023; Accepted 19 January 2024
Available online 20 January 2024

propagation losses and shadowing in indoor environments. In [12] authors present the design, implementation, and validation of a phase-compensated channel sounder that can support the virtual antenna array (VAA) scheme and long-range measurements at W bands (i.e., 75–110 GHz). Additionally, in [13] a state-of-art long-range 28 GHz and 300 GHz vector network analyzer (VNA) based channel sounder using optical cable solutions, is presented which can support a measurement range up to 300 m and 600 m in principle. In [14] the most commonly employed small-scale distributions to model the small-scale fading amplitude have been estimated from multiple-input multiple-output (MIMO) measurements conducted in a lab at the 94 GHz band with line-of-sight (LOS) condition for vertical (VV) and horizontal (HH) polarization combination.

Hence, more channel measurements and other efforts will be necessary to gain a better knowledge of the channel parameters in indoor environments at 94 GHz (delay spread, maximum excess delay (MED), coherence bandwidth, etc.). Thus, in this paper, an extensive measurement campaign is carried out to measure the MIMO channel transfer functions at 94 and 60 GHz in a laboratory. The values of the relative received power, root mean square (RMS) delay spread, maximum excess delay and coherence bandwidth at 94 GHz are compared both for VV and HH polarization, and the results are compared with those obtained in the 60 GHz band. As far as the authors are concern, there is not much information in the literature comparing from an experimental point of view these two frequency bands.

The paper is organized as follows. Section 2 describes the experimental setup and the channel sounder. Section 3 gives an overview of the studied parameters. The relative received power, RMS delay spread, maximum excess delay and coherence bandwidth are presented and discussed in Section 4. Finally, our conclusions are presented in Section 5.

2. Experimental setup

2.1. Scenario

The measurement scenario was a laboratory located on the first floor of the Universidad Politécnica de Cartagena research building (Spain). A complete description of the scenario is given in [15]. Fig. 1 shows the measurement scenario and the 14 transmitting positions at 94 GHz. The distance between each receiver (Rx) position and the transmitter (Tx) is indicated in the Table 1. In all the experiments, a LOS existed for all positions. In seven of the positions, measurements were taken in both the 94 and 60 GHz bands, and these positions are shown in gray in Fig. 1 (positions 4, 5, 8, 9, 10, 11, 14). The reason for the larger number of data points for 94 GHz is that setting up at 94 GHz involved separating the upconverters (heads), which required 8.5 m cables [16]. In other words, the signals in the converter operated at 20 GHz, whereas at 60 GHz the frequency was three times greater, and it was not possible to take measurements over longer distances.

2.2. Measurements

To measure the channel transfer function, a commercial vector network analyzer (VNA) was used (model R&S ZVA 67 from Rohde & Schwarz). To acquire multiple antennas, the Tx and Rx antennas were virtually repositioned using two different array configurations involving a uniform rectangular array (URA) and a uniform linear array (ULA) for the Tx and Rx, respectively. In [15] a complete description of the configurations is given. For the ULA, five elements were uniformly spaced along the Y-direction, whereas for the URA a 6×6 uniform rectangular grid. A total of 180 Tx_{ULA}/Rx_{URA} combinations massive MIMO (mMIMO) measurements were performed. The separation between antenna elements for both the URA Tx and the ULA Rx was set to 1 mm for the 94 GHz band ($<\lambda_{94GHz}/2$) and 2 mm for the 60 GHz band ($<\lambda_{60GHz}/2$).

For the measurements at 94 GHz, the measured frequency range was 92.5 – 95.5 GHz, using 1024 frequency points. The R&SZVA-Z110E converter (W-band WR-10, 75–110 GHz) was used for both the transmitting and the receiving units. The measured dynamic range for an intermediate frequency of 10 Hz was 107 dB and the VNA output power was 10 dBm in the converter. Both the Tx and Rx used identical polarimetric omni-directional antennas, manufactured by Mi-Wave (WR-10). These antennas had a gain of 2 dB and had a 30° aperture in the vertical plane. Two combinations of polarization measurements were executed, allowing for horizontal Tx and horizontal Rx (HH) as well as vertical Tx and vertical Rx (VV) configurations.

For the measurements at 60 GHz, the measured frequency range was 57 – 66 GHz, using 2048 frequency points. Coaxial cables were used to separate the Tx and Rx. These cables had insertion losses of approximately 5 dB/m at 62 GHz, which was compensated using two amplifiers (model HXI HLNA-465) with 25 dB gain. The measured dynamic range for an intermediate frequency of 10 Hz was 90 dB and the VNA output power was 5 dBm. Two identical vertically polarized omni-directional antennas (Q-par QOM55-65 VRA) were used at the transmitting and receiving ends, which had a gain in the range 4.3–5.2 dB across the frequency band of interest. Their typical 3 dB elevation beamwidth ranged from 24 to 33°, and they provided omni-directional coverage in the horizontal plane. Within this frequency band, only one polarization combination was considered, and all measurements were conducted using the VV configuration.

In both frequency bands, the system was 'through' calibrated to eliminate the impact of cables or amplifiers, thus ensuring that the VNA accurately assessed the radio channel between the antennas.

3. Channel characteristics

For each frequency band, the relative received power, the RMS delay spread, the maximum excess delay and the coherence bandwidth were

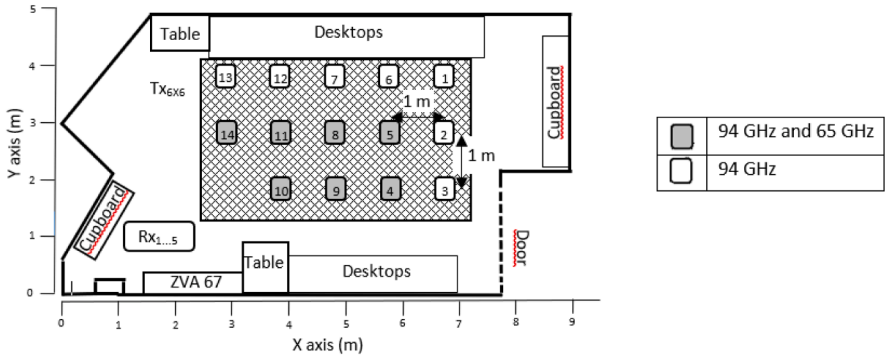

Fig. 1. Location of Tx and Rx in the laboratory.

Table 1
Distances between transmitting and receiving antennas for each Rx position.

Rx Position	14	10	11	13	12	9	8	7	4	5	6	3	2	1
Tx-Rx Distance (m)	1.4	1.9	2.2	2.3	2.8	2.8	3.1	3.6	3.9	4.0	4.3	4.9	5.1	5.4

calculated.

3.1. Relative received power

The relative received power (Pr) for each Tx-Rx distance was computed based on the value of H obtained from the measurements and averaged over the number of frequency samples and 180 Tx_{ULA}/Rx_{URA} combinations. It can be expressed in logarithmic units as follows [17]:

$$Pr(d) = 10\log_{10}\left(\frac{1}{N_f N_c}\sum_{n=1}^{N_f}\sum_{m=1}^{N_c}|H(f_n, c_m, d)|^2\right) \quad (1)$$

where d is the corresponding Tx-Rx distance, N_f is the number of frequency samples considered in each band, N_c is the number of Tx_{ULA}/Rx_{URA} combinations, and || indicates the absolute value.

3.2. RMS delay spread

An understanding of the characteristics of a channel's time dispersion is valuable in terms of enhancing wireless system designs. The key metric for characterizing this time dispersion is the RMS delay spread, denoted as τ_{rms}. This parameter, derived from the second-order central moment of the power delay profile (PDP), is the most widely used descriptor of time dispersion in wireless channels, and is defined as [17]. All of the multipath components of the PDP within 20 dB of the maximum are included.

3.3. Maximum excess delay

To calculate the MED for the power delay profile, a power threshold is set, which is defined as the maximum power in the PDP minus X dB. A typical value is 20 dB [18]. Hence, the MED is the difference between the last delay for which the power in the PDP is above the threshold and the instant at which the first signal arrives.

3.4. Coherence bandwidth

The coherence bandwidth (B_c) is calculated from the frequency response of the channel as the maximum separation between two frequency components (Δf) at which a certain threshold of correlation is maintained, typically 0.9 (90 %). The autocorrelation function for the envelope signals is calculated as in [19]. The 90 % coherence bandwidth is denoted as $B_{c,90\%}$.

4. Results and discussion

In this section, we present the parameters described above. The results are analyzed at 94 GHz for both vertical and horizontal polarization, and the results obtained at 94 and 60 GHz are compared.

4.1. Performance at 94 GHz

Table 2 shows the values of the parameters obtained for each polarization. The mean and standard deviation (STD) are also shown for all parameters. The 14 positions are displayed in ascending order in terms of the Tx-Rx distance. Note that for each Tx-Rx distance, 180 Tx_{ULA}/Rx_{URA} combinations are averaged.

4.1.1. Relative received power and RMS delay spread

As shown in Table 2, the mean value of P_r for all the distances was very similar for both polarizations, and it was on the order of − 87 dB. The STD values for P_r were 2.63 dB and 3.35 dB for horizontal and vertical polarization, respectively. Fig. 2 shows the mean P_r for each Tx-Rx distance, and it can be seen that it tends to decrease as the Tx-Rx distance increases. To illustrate this effect more clearly, we show the regression line obtained from the floating-intercept (FI) model [20]. The FI model is defined by β, α and χ_σ^{FI}. Where β is the FI parameter (offset term), and α is the path loss exponent. χ_σ^{FI} represents the shadowing loss, and is characterized by a standard deviation σ.

In Fig. 2, dashed lines obtained from the FI model are shown for both polarizations. A steeper slope is observed for VV polarization, with a value of 1.83, whereas for HH polarization the slope is 1.55 (see Table 3). Similar results were reported in [21] for 80 GHz, with values of 1.47 for an office and 1.67 for a conference room. The authors of [10] and [11] reported results of 1.8 and 1.5, respectively, for 94 GHz in a similar room. Finally, it can be observed that at greater distances, the P_r tends to converge in both horizontal and vertical polarization.

Regarding the τ_{rms} in Table 2, the results obtained for both the VV and HH polarizations demonstrate that the temporal dispersion is low, as the maximum values obtained are 7.77 and 9.68 ns, respectively. It

Table 2
Parameters for each polarization at 94 GHz.

Tx-Rx distance (m)	Pr (dB)		τ_{rms} (ns)		MED (ns)		$B_{c,90\%}$ (MHz)	
	VV	HH	VV	HH	VV	HH	VV	HH
1.46	−82.10	−86.62	4.30	4.15	23.00	26.29	33.40	21.60
1.95	−85.61	−82.56	3.91	2.52	23.75	22.34	26.70	35.53
2.25	−83.55	−88.32	1.52	4.87	18.59	36.26	32.00	10.80
2.33	−87.34	−80.55	7.77	0.70	48.32	12.93	17.90	37.00
2.87	−86.42	−88.12	3.72	2.81	35.60	33.05	17.10	29.96
2.89	−86.16	−85.06	4.30	2.21	31.43	29.48	26.00	25.60
3.14	−88.95	−91.80	7.34	9.68	48.24	50.34	19.60	10.40
3.68	−87.28	−89.41	4.11	6.04	35.42	42.14	23.60	18.60
3.92	−87.97	−89.03	4.73	7.19	33.67	40.12	22.70	20.50
4.09	−90.90	−92.92	7.25	8.44	42.03	65.45	15.70	10.40
4.38	−89.53	−89.42	5.40	4.25	41.26	36.41	20.60	20.10
4.92	−89.36	−87.97	6.25	5.15	38.67	37.91	19.90	21.30
5.14	−90.49	−89.91	6.04	5.27	43.33	43.85	20.40	23.90
5.49	−90.46	−89.89	5.25	4.08	44.46	38.44	17.60	20.80
Mean	−87.58	−87.97	4.14	4.88	36.27	36.79	22.36	22.13
STD	2.63	3.35	1.69	2.39	9.39	12.57	5.42	8.78

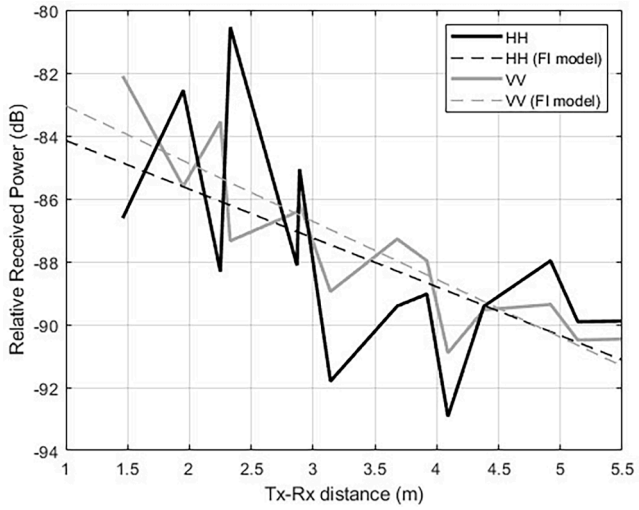

Fig. 2. Relative received power for VV and HH polarization at 94 GHz.

Table 3
Parameters of the FI model for VV and HH polarization.

β		α		σ	
VV	**HH**	**VV**	**HH**	**VV**	**HH**
81.2	82.60	1.83	1.55	2.15	3.14

shows that the mean value of τ_{rms} is very similar for both polarizations, with an average across all distances of 4.88 ns for VV polarization and 4.14 ns for HH polarization. The STD values are 1.69 and 2.39 ns for VV and HH polarization, respectively. There is clearly no relationship between these values and the Tx-Rx distance. From Fig. 3, which shows the CCDF, it can be observed that for a probability of 0.8, the τ_{rms} obtained is 1 ns greater when VV polarization is used compared to HH polarization. This indicates that values greater than 7 ns are obtained with a probability of less than 0.3 for both polarizations, although they are more likely when using the HH polarization.

4.1.2. Maximum excess delay

From Table 2, it can be observed that the mean values of MED for VV and HH polarization are very similar, at 36.27 ns and 36.79 ns, respectively. However, the STD values are 12.57 ns and 9.39 ns for HH and VV polarization, respectively.

We focus on the CCDF to carry out a more detailed analysis (see Fig. 4). It can be observed that the behavior in both polarizations is nearly identical in the range 25–45 ns.

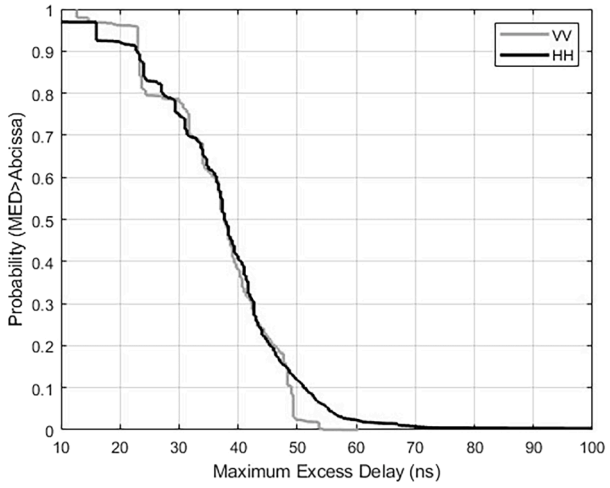

Fig. 4. CCDF for maximum excess delay at 94 GHz, for VV and HH polarization.

4.1.3. Coherence bandwidth

The minimum, maximum, mean and standard deviation values of $B_{c,90\%}$ are given in Table 2. The values of the coherence bandwidth had a higher dispersion for HH polarization, and $B_{c,90\%}$ ranged from 10.40 to 38.80 MHz, with a mean value of 22.13 MHz. For VV polarization, the maximum value of $B_{c,90\%}$ was on the order of 33.40 MHz. The difference between the mean values for HH and VV polarizations was not high (about 0.23 MHz), with a greater value for VV polarization.

In Fig. 5, $B_{c,90\%}$ obtained as a function of the Tx-Rx distance is shown for both HH and VV polarizations at 94 GHz. It can be observed that the $B_{c,90\%}$ values are more scattered at distances of less than 3.5 m, especially in HH polarization. However, above this distance, the results converge around the mean values of 22.13 MHz and 22.36 MHz for the HH and VV polarizations, respectively. The mean square error (MSE) approximation is shown for both polarizations (dashed lines). When using VV polarization, the average $B_{c,90\%}$ values decrease with a steeper slope compared to HH polarization. Regarding the variance among the values averaged at each Tx-Rx distance, no clear relationship is observed for either of the two polarizations.

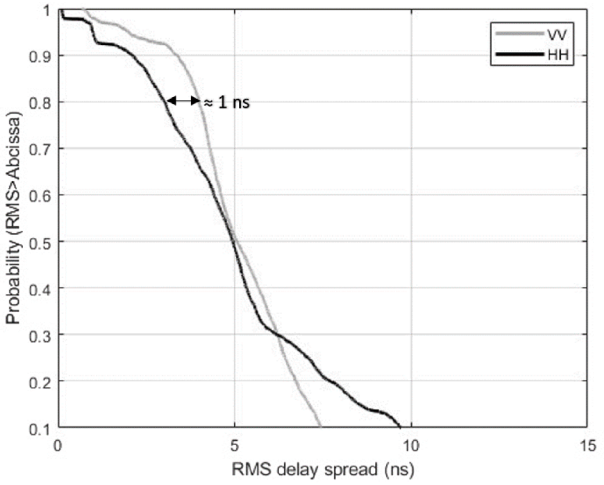

Fig. 3. CCDF for the RMS delay spread for VV and HH polarization at 94 GHz.

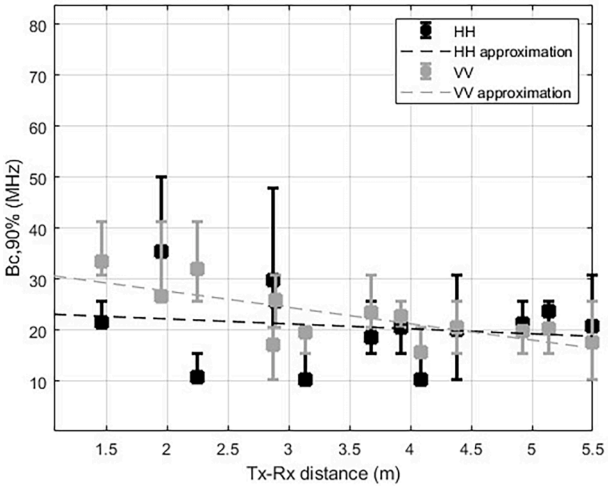

Fig. 5. Coherence bandwidth at 94 GHz for VV and HH polarization.

4.2. Comparison of the 94 and 60 GHz bands

In Fig. 1, seven positions are marked in gray (positions 4, 5, 8, 9, 10, 11, 14). Measurements were taken at these positions in both the 94 and 60 GHz bands.

The results at 60 GHz were compared with those obtained at 94 GHz for VV polarization. This polarization was chosen because better results were obtained when comparing the previous results.

Table 4 displays the values for the relative received power, RMS delay spread, MED and coherence bandwidth deduced from the measurements at 60 and 94 GHz.

4.2.1. Relative received power

From Table 4, we can observe the changes in the mean received power at 94 and 60 GHz with the Tx-Rx distance. The analysis indicates that the power was higher in the 60 GHz band, with values of − 72.08 dB at 1.46 m and − 79.32 dB at 4.09 m. The mean values were − 76.75 and − 86.46 dB at 60 and 94 GHz, respectively. From the plot of CCDF in Fig. 6, we see that the ratio Pr_{60GHz}/Pr_{94GHz} reaches 9.8 dB close to the mean values. This value considers both the frequency difference and the antenna patterns. Considering free space and that the frequency response obtained in the measurements includes the antenna gains ($G_{60GHz} = 5$ dB, $G_{94GHz} = 2$ dB), the theoretical ratio Pr_{60GHz}/Pr_{94GHz} is calculated as 9.9 dB using the expression in (2), according to Friis. Hence, the values from theory and measurement are very similar.

$$Pr_{60GHz}/Pr_{94GHz} = 20log_{10}(94GHz/60GHz) + 2G_{60GHz} - 2G_{94GHz} \quad (2)$$

4.2.2. RMS delay spread

The mean RMS delay spread obtained at each Tx-Rx distance is shown in Fig. 7. In general, the τ_{rms} obtained at 94 GHz is higher than at 60 GHz. In the 94 GHz band, a increasing trend with Tx-Rx distance is observed: the minimum τ_{rms} is 1.52 ns at a distance of 2.25 m, and the maximum value is 7.25 ns at 4.09 m. However, in the 60 GHz band, no clear relationship with distance is observed. To enable a comparison of both bands, we present the mean and STD values in Table 4. In the 60 GHz band, the results are 2.23 ns and 1.23 ns, respectively, while at 94 GHz, they are 4.77 ns and 2.02 ns, respectively. It is worth noting that the values of τ_{rms} derived here were lower than those published in [22] for an entire laboratory at 60 GHz, where the values covered the range 4.28–35.92 ns. In [23], mean τ_{rms} values were obtained as 0.68, 3.78 and 3.59 ns for a meeting room, a computer laboratory and a classroom, respectively. Values ranging from 3 to 15 ns and 2–12 ns were also obtained at 70 GHz in an office and a shopping mall, respectively, as reported in [24]. A mean value of 3.30 ns was measured in a typical office at 73 GHz [19]. In [21], a mean τ_{rms} value of 6.1 ns was obtained for an office at 82 GHz.

4.2.3. Maximum excess delay

From Table 4, it can be observed that the values of MED are lower at 60 GHz. It shows that the mean value of MED obtained at 94 GHz is 31.53 ns, whereas at 60 GHz, it is 20.92 ns. Furthermore, the standard deviation at 94 GHz is 10.76 ns, while at 60 GHz, it is 6.83 ns.

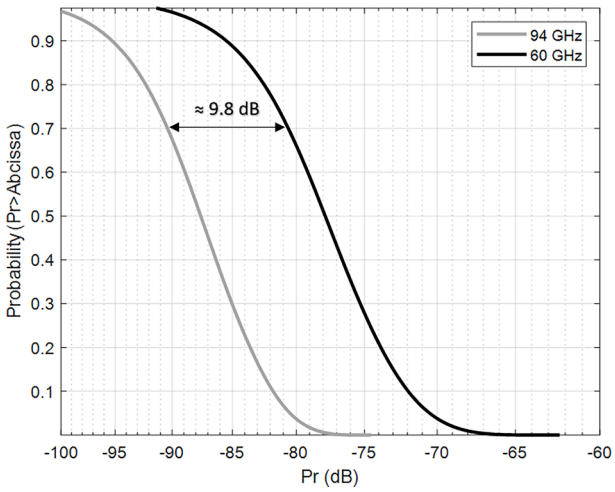

Fig. 6. CCDF of the relative received power at 94 and 60 GHz.

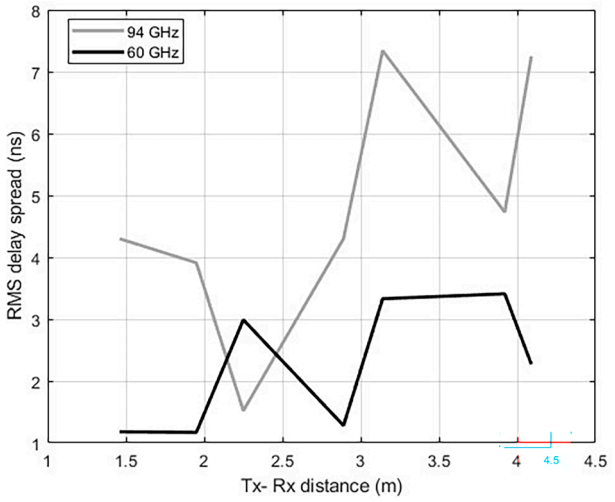

Fig. 7. RMS delay spread at 94 and 60 GHz.

4.2.4. Coherence bandwidth

When comparing the $B_{c,90\%}$ obtained at 94 GHz with that obtained at 60 GHz, we see from Fig. 8 that when the Tx-Rx distance is less than 2 m, a higher $B_{c,90\%}$ is achieved at 60 GHz. At a Tx-Rx distance of 1.4 m, a $B_{c,90\%}$ value of 38.77 MHz is obtained at 60 GHz, while at 94 GHz, a value of over 33.40 MHz is achieved. However, we note that above 2 m, the $B_{c,90\%}$ is higher at 94 GHz. At the maximum distance of 4.1 m using 94 GHz, a value of 15.70 MHz is reached, while at 60 GHz, a value of

Table 4
Parameters at 60 and 94 GHz.

Tx-Rx distance (m)	Pr (dB)		τ_{rms} (ns)		MED (ns)		B_c (MHz)	
	60 GHz	94 GHz	60 GHz	94 GHz	60 GHz	94 GHz	60 GHz	94 GHz
1.46	−72.08	−82.10	1.18	4.36	11.77	23.00	38.77	33.40
1.95	−72.57	−85.61	1.17	3.91	14.53	23.75	38.11	26.70
2.25	−77.88	−83.55	2.99	1.52	28.90	18.59	12.09	32.00
2.89	−77.08	−86.16	1.28	4.30	15.37	31.43	16.38	26.00
3.14	−78.26	−88.95	3.33	7.34	23.81	48.24	11.58	19.60
3.92	−80.08	−87.97	3.41	4.73	26.22	33.67	9.02	22.70
4.09	−79.32	−90.90	2.27	7.25	25.85	42.03	8.99	15.70
Mean	−76.75	−86.46	2.23	4.77	20.92	31.53	19.28	25.15
STD	3.17	3.06	1.02	2.02	6.83	10.76	13.32	6.36

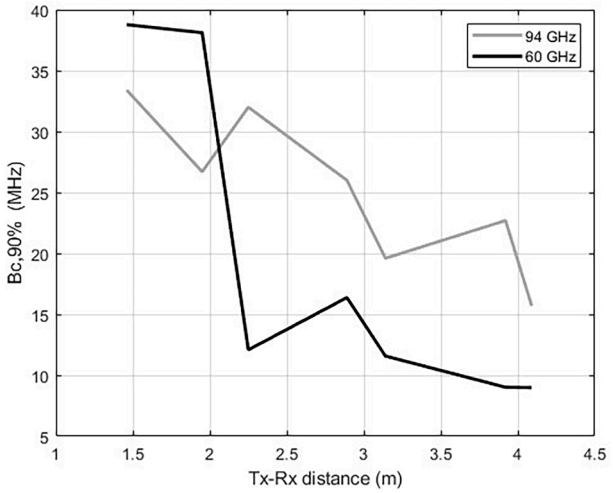

Fig. 8. Coherence bandwidth at 94 GHz and 60 GHz.

8.99 MHz is obtained. Hence, a decreasing trend in $B_{c,90\%}$ with the Tx-Rx distance is observed. The mean values are shown in Table 4 as 19.28 and 25.15 MHz at 60 and 94 GHz, respectively. These values fall within the ranges obtained in [22] at 60 GHz in a laboratory environment, where the mean value was 19.08 MHz and the minimum and maximum were 3.77 and 49.37 MHz for Tx-Rx distances of 17 and 1.5 m, respectively. The obtained values are fairly low because the chosen correlation threshold was 0.9; with a lower threshold, the $B_{c,90\%}$ values would be higher.

5. Conclusions

In this paper, experimental results in the W band are presented and compared to similar ones obtained at 60 GHz. The relative received power, RMS delay spread, MED, and coherence bandwidth characteristics of the propagation channel in a laboratory environment were analyzed from a channel measurement campaign carried out at 60 and 94 GHz. The channel measurements were performed under LOS conditions, and were performed for HH and VV polarization. The results obtained for both polarizations were similar, with the average received power, the mean RMS delay spread, the mean MED, and the mean coherence bandwidth in both polarizations being on the order of − 87 dB, 4.5 ns, 36.5 ns and 22 MHz, respectively. We found that the STD was always greater for HH polarization. For the MED and the coherence bandwidth, the STD values were 3.18 ns and 3.36 MHz, respectively, greater when HH polarization is used compared to VV polarization.

The ratio Pr_{60GHz}/Pr_{94GHz} reached a value of 9.8 dB, coinciding with Friis. For the mean RMS delay spread, values of 2.23 and 4.77 ns were obtained for the 60 and 94 GHz bands, respectively. The mean value of MED obtained at 94 GHz was 31.53 ns, whereas at 60 GHz, it was 20.92 ns. Finally, the mean $B_{c,90\%}$ was found to be 19.28 and 25.15 MHz at 60 and 94 GHz, respectively. We note that all values except the received power were higher at 94 GHz.

The results reported in this paper will enable a better knowledge of the propagation characteristics in laboratory environments, based on new measurements at 94 GHz. They can be used to improve the design and evaluate the performance of future 6G networks in these scenarios. In future work, it would be interesting to study the parameters described here for a non-line-of-sight context within the same laboratory.

CRediT authorship contribution statement

Concepción Sanchis-Borrás: Writing – review & editing, Writing – original draft, Validation, Software, Resources, Methodology, Investigation, Formal analysis, Data curation, Conceptualization. **María-Teresa Martínez-Inglés:** Writing – original draft, Supervision, Methodology, Investigation, Data curation. **José-Víctor Rodríguez:** Writing – review & editing, Visualization, Validation, Supervision, Investigation, Funding acquisition, Formal analysis. **José-Maria Molina-Garcia-Pardo:** Writing – review & editing, Validation, Supervision, Resources, Project administration, Investigation, Funding acquisition, Formal analysis, Conceptualization.

Declaration of competing interest

The authors declare that they have no known competing financial interests or personal relationships that could have appeared to influence the work reported in this paper.

Data availability

Data will be made available on request.

Acknowledgments

The authors are grateful to the Ministerio de Ciencia e Innovación of the Spanish Government for co-funding this research under the National Project PID2022-136869NB-C32.

References

[1] David K, Berndt H. 6G vision and requirements: Is there any need for beyond 5G? IEEE Veh Technol Mag 2018;13:72–80.
[2] Al-Saman A, Cheffena M, Elijah O, Al-Gumaei YA, Abdul Rahim SK, Al-Hadhrami T. Survey of millimeter-wave propagation measurements and models in indoor environments. Electronics 2021;10:1653.
[3] Martinez-Ingles M-T, Gaillot DP, Pascual-Garcia J, Molina-Garcia-Pardo J-M, Rodríguez J-V, Rubio L, et al. Channel sounding and indoor radio channel characteristics in the W-band. EURASIP. J Wirel Com Network 2016;2016(1). https://doi.org/10.1186/s13638-016-0530-7.
[4] Moraitis N, Constantinou P. Measurements and characterization of wideband indoor radio channel at 60 GHz. IEEE Trans Wirel Commun 2006;5:880–9.
[5] Bamba, A.; Mani, F.; D'Errico, R. A comparison of indoor channel properties in V and E bands. In 2017 11th European Conference on Antennas and Propagation (EUCAP), Paris, France, 2017, pp. 3361-3365. doi: 10.23919/EuCAP.2017.7928448.
[6] World Radiocommunication Conference 2019 (WRC-19), Sharm el-Sheikh, Egypt, 28 October–22 November 2019, p. 374.
[7] Rajatheva, N. et al. 6G White Paper on Broadband Connectivity in 6G. [Internet]. June 2020. Available from: https://arxiv.org/abs/2004.14247.
[8] Tripathi, S.; Sabu, N.V.; Gupta, A.K.; Dhillon, H.S. Millimeter-wave and terahertz spectrum for 6G Wireless. In 6G Mobile Wireless Networks. Computer Communications and Networks; Wu Y. et al. (eds); Springer, 2021.
[9] ITU-R, draft new recommendation. Framework and overall objectives of the future development of IMT for 2030 and beyond. June 2023.
[10] Kajiwara, A. Indoor propagation measurements at 94 GHz. In Proc. 6th International Symposium on Personal, Indoor and Mobile Radio Communications-PIMRC, 1995, vol. 3, pp. 1026-1030. doi:10.1109/PIMRC.1995.477099.
[11] Helminger, J.; Detlefsen, J.; Groll, H. Propagation properties of an indoor-channel at 94 GHz. In Proc. ICMMT International Conference on Microwave and Millimeter Wave Technology, Beijing, 1998, pp. 9-14. doi:10.1109/ICMMT.1998.768215.
[12] Lyu Y, Yuan Z, Zhang F, Kyösti P, Fan W. Virtual antenna array for W-band channel sounding: Design, implementation, and experimental validation. IEEE J Sel Top Signal Process 2023;17(4):729–44. https://doi.org/10.1109/JSTSP.2023.3301135.
[13] Bengtson M, Lyu Y, Fan W. Long-range VNA-based channel sounder: Design and measurement validation at MmWave and sub-THz frequency bands. China Commun 2022;19(11):47–59. https://doi.org/10.23919/JCC.2022.11.004.
[14] Reig J, Martinez-Ingles MT, Molina-Garcia-Pardo JM, Rubio L, Rodrigo-Peñarrocha VM. Small-scale distributions in an indoor environment at 94 GHz. Radio Sci 2017;52:852–61. https://doi.org/10.1002/2017RS006335.
[15] Sanchis-Borrás C, Martínez-Inglés M-T, Molina-García-Pardo J-M, García JP, Rodríguez J-V. Experimental study of MIMO-OFDM transmissions at 94 GHz in indoor environments. IEEE Access 2017;5:7488–94.
[16] Martinez-Ingles M-T, Gaillot DP, Pascual-Garcia J, Molina-Garcia-Pardo J-M, Rodríguez J-V, Rubio L, et al. Channel sounding and indoor radio channel characteristics in the W-band. J Wirel Com Network 2016;2016(1). https://doi.org/10.1186/s13638-016-0530-7.
[17] Rappaport, T.S. Wireless Communications: Principles and Practice; Prentice Hall: Upper Saddle River, NJ, USA, 2002.
[18] Al-Samman, A.M.; Azmi, M.H.; Al-Gumaei, Y.A.; Al-Hadhrami, T.; Abd. Rahman, T.; Fazea, Y.; Al-Mqdashi, A. Millimeter wave propagation measurements and characteristics for 5G system. Appl. Sci. 2020, 10, 335.

[19] Howard SJ, Pahlavan K. Autoregressive modeling of wide-band indoor radio propagation. IEEE Trans Commun 1992;40:1540–52.
[20] Deng, S.; Samimi, M.K.; Rappaport; T.S. 28 GHz and 73 GHz millimeter-wave indoor propagation measurements and path loss models. In IEEE International Conference on Communications Workshops (ICCW), London, UK, 2015, pp. 1244-1250.
[21] Bamba, A.; Mani, F.; D'Errico, R. E-band millimeter wave indoor channel characterization. In 2016 IEEE 27th Annual International Symposium on Personal, Indoor, and Mobile Radio Communications (PIMRC), Valencia, Spain, 2016, pp. 1-6. doi: 10.1109/PIMRC.2016.7794729.
[22] Pekou, A.; Nastos, V.; Moraitis, N.; Constantitiou, P. Time delay and coherence bandwidth measurements at 60 GHz in an indoor environment for WLANs. In IEEE 59th Vehicular Technology Conference, Milan, Italy, 2004, Vol.1, pp. 93-97. doi: 10.1109/VETECS.2004.1387919.
[23] Al-jzari, A.; Towers, J.; Salous, S. Characterization of indoor environment in the 60 GHz band. In XXXIII General Assembly and Scientific Symposium of the International Union of Radio Science, Rome, Italy, 2020, pp. 1-4.
[24] Haneda, K.; Järveläinen, J.; Karttunen, A.; Kyrö, M.; Putkonen, J. Indoor short-range radio propagation measurements at 60 and 70 GHz. In 8th European Conference on Antennas and Propagation (EuCAP2014), The Hague, Netherlands, 2014, pp. 634-638. doi: 10.1109/EuCAP.2014.6901839.